Processing and Application of Ceramics 9 [1] (2015) 1–9
DOI: 10.2298/PAC1501001G

Effect of Ni/Nb on structure, electrical and ferroelectric properties of 0.5PNN-0.5PZT ceramics

Rashmi Gupta, Seema Verma, Deepa Singh, Karan Singh, Krishen K. Bamzai*

Crystal Growth & Materials Research Laboratory, Department of Physics and Electronics, University of Jammu, 180006 Jammu, India

Received 11 November 2014; Received in revised form 17 January 2015; Received in revised form 20 February 2015; Accepted 23 February 2015

Abstract

The solid solutions of lead nickel niobate (PNN) and lead zirconate titanate (PZT), with general formula 0.5 $Pb(Ni_xNb_{1-x})O_3$-0.5 PZT, where x = 1/3, 1/2 and 2/3 and Zr/Ti = 50/50, were prepared by conventional solid state reaction technique. The perovskite phase formation and morphology were examined by powder X-ray diffraction (XRD) and scanning electron microscopy (SEM) techniques. From microstructure investigations, the grain size was found to lie in the range of 0.2–1.1 μm. Diffuse phase transition and dielectric relaxation was obtained for all three compositions. The nature of dielectric relaxation was investigated through complex plane Argand plot or Cole-Cole plot. It was found that both grains as well as grain boundary contribute to dielectric relaxation. A direct correlation between the grain size and electrical properties was obtained. The remnant polarization and grain size were found to follow the inverse relationship. The inverse relationship between remnant polarization and grain size was established.

Keywords: *PNN-PZT composites, solid state synthesis, XRD, SEM, dielectric and ferroelectric properties*

I. Introduction

Complex perovskite type $AB'B''O_3$ structure show excellent dielectric, ferroelectric and electromechanical properties that opened a wide field of applications such as sensors, actuators, multilayer capacitors, transducers, memory devices etc. [1–4]. The highly tolerant $AB'B''O_3$ structure provides enough scope for modification either at A-site or B-site. The electrical properties and ferroelectric phase transition temperature can be effectively controlled by suitable doping at B-site. Lead zirconate titanate (PZT), a normal ferroelectric material, is found to possess excellent dielectric and piezoelectric properties for compositions near the morphotrophic phase boundary (MPB) located around Zr : Ti~1 : 1 separating Zr-rich rhombohedral phase from Ti-rich tetragonal phase [5]. Lead nickel niobate (PNN) is a relaxor ferroelectric and possesses a broad dielectric peak unlike that in PZT, which is a normal ferroelectric with a sharp dielectric peak. Thus, by controlling the amount of PZT, the Curie temperature in PNN-PZT can be engineered over a wide temperature range. A number of researchers [6–9] have carried out investigations on such binary systems being relaxor or normal ferroelectric with optimum dielectric permittivity and piezoelectric properties. Some compositions in the ternary solid solution of $Pb(Ni_{1/3}Nb_{2/3})O_3$-$PbZrO_3$-$PbTiO_3$ (PNN-PZ-PT) might have large electromechanical coupling factor (k_p > 65%) and high dielectric constant (ε_r > 5000) [10,11]. A detailed investigation on the reaction kinetics of $Pb(Ni_{1/3}Nb_{2/3})O_3$-$Pb(Zr_{0.48}Ti_{0.52})O_3$ using conventional solid state reaction technique was carried out by Babushkin *et al.* [12] in which the presence of various pyrochlore phases at different temperatures was detected. Choi *et al.* [13] investigated the effect of NiO addition to the PNN-PZT ceramics on piezoelectric properties and it was found that addition of 1 mol% of NiO into PNN-PZT caused an abrupt increase in dielectric and piezoelectric properties. These investigations were concentrated on the addition of NiO in different mole percent to the PNN-PZT ceramics and as such there are no detailed results related to ferroelectric properties. However, in the present work, both NiO and Nb_2O_5 were varied alternatively with different compositions. Hence, in the present investigation, solid solutions of a relaxor ferro-

*Corresponding author: tel/fax: +91 191 2450939,
e-mail: *kkbamz@yahoo.com*

electric (PNN) and a normal ferroelectric (PZT) were prepared with general formula $0.5\,Pb(Ni_xNb_{1-x})O_3$-$0.5\,PZT$, where x = 1/3, 1/2 and 2/3 and Zr/Ti = 50/50. The compositions prepared in the present investigation are $0.5\,Pb(Ni_{1/3}Nb_{2/3})O_3$-$0.5\,Pb(Zr_{1/2}Ti_{1/2})O_3$ (denoted with PNN(1/3)-PZT), $0.5\,Pb(Ni_{1/2}Nb_{1/2})O_3$-$0.5\,Pb(Zr_{1/2}Ti_{1/2})O_3$ (denoted with PNN(1/2)-PZT) and $0.5\,Pb(Ni_{2/3}Nb_{1/3})O_3$-$0.5\,Pb(Zr_{1/2}Ti_{1/2})O_3$ (denoted with PNN(2/3)-PZT). To the best of authors' knowledge, there is no such report on the effect of change in the nickel/niobium content on the structural, electrical and ferroelectric properties of PNN-PZT composite system.

II. Experimental

The solid solutions of lead nickel niobate (PNN) and lead zirconate titanate (PZT) with general formula $0.5\,Pb(Ni_xNb_{1-x})O_3$-$0.5\,PZT$, where x = 1/3, 1/2 and 2/3 and Zr/Ti = 50/50 were prepared by conventional solid state reaction technique. The starting powders of PbO, NiO, Nb_2O_5, ZrO_2 and TiO_2 (S D Fine - Chem Limited of 99% purity) were weighed and uniformly mixed in the stoichiometric ratio according to three chemical formulas, $0.5\,Pb(Ni_{1/3}Nb_{2/3})O_3$-$0.5\,Pb(Zr_{1/2}Ti_{1/2})O_3$, $0.5\,Pb(Ni_{1/2}Nb_{1/2})O_3$-$0.5\,Pb(Zr_{1/2}Ti_{1/2})O_3$ and $0.5\,Pb(Ni_{2/3}Nb_{1/3})O_3$-$0.5\,Pb(Zr_{1/2}Ti_{1/2})O_3$. The mixture was then ball milled, dried and calcined at 900 °C for 2 h. The powder obtained after calcination was again ground and mixed with 5 wt.% of polyvinyl alcohol as a binder and isostatically pressed in the form of circular disks and then sintered at 1100 °C with a heating/cooling rate of 4 °C/min with a dwell time of 4 h.

Structural characterization of the sintered samples was carried out using Rigaku X-ray diffractometer with monochromatic CuK_α radiation (λ = 1.5405 Å) and nickel filter in a wide 2θ range of 20–80° using step scanning with a step size of 0.02°. The percentage of perovskite phase content was calculated using equation [14]:

$$P_{perov} = 100\frac{I_{110}}{I_{110} + I_{pyro}} \quad (1)$$

where I_{110} and I_{pyro} are intensities of the most intensive perovskite and pyrochlore XRD peaks, respectively. Scanning electron microscope (SEM, JEOL JSM-6390 LV) was used to examine the surface morphology and grain size whereas chemical composition was confirmed by energy dispersive X-ray analysis (EDAX, JEOL JED-2300). For electrical measurements, parallel plate capacitor was prepared by applying silver paste on both sides of the sintered pellet and firing at 400 °C for 1 h. The dielectric measurements were recorded with the help of automated impedance analyser (4192A LF model) interfaced with USB-GPIB converter 82357 (Agilent) and further automated by using a computer for data recording, storage and analysis. The polarization versus electric field (*P-E* hysteresis loops) measurement at room temperature was carried out by using an automatic *P-E* loop tracer (Marine India Electrocom Ltd., New Delhi, India).

III. Results and discussion

3.1. Structural and morphological studies

Figure 1 shows the X-ray diffraction pattern for three different compositions of $0.5\,Pb(Ni_xNb_{1-x})O_3$-$0.5\,PZT$, where x = 1/3, 1/2 and 2/3. These diffraction peaks were matched and indexed according to JCPDS Card 34-0103 for $Pb(Ni_{0.33}Nb_{0.67})O_3$ having space group *Pm3m* and 73-2022 for $Pb(Zr_{0.58}Ti_{0.42})O_3$ with space group *R3m*. The diffraction patterns show that apart from the formation of perovskite phase, an undesirable pyrochlore phase appears (Fig. 1).

Only the sintered PNN(1/3)-PZT ceramics possess 100% perovskite phase, as is clearly seen in Fig. 1a. On increasing the value of x, the pyrochlore phase content increases and maximal amount is present in the sample PNN(2/3)-PZT (Fig. 1c). The increase in pyrochlore phase with increase in nickel concentration is due to the off-stoichiometry of cations on the B-site which resulted in the creation of vacancies and hence the pyrochlore phase formation.

Table 1 gives the data regarding percentage of perovskite phase, theoretical density and grain size for all three compositions. Theoretical density was calculated from weight and volume of the sample.

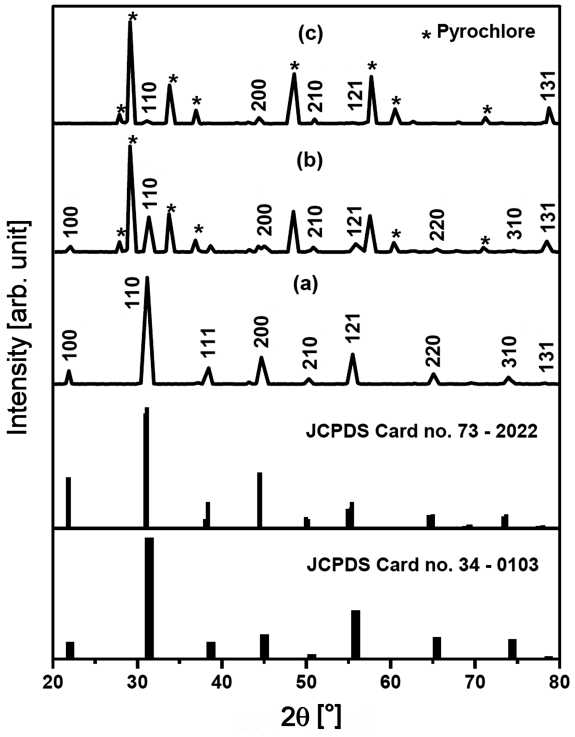

Figure 1. Room temperature X-ray diffraction pattern of: a) PNN(1/3)-PZT, b) PNN(1/2)-PZT and c) PNN(2/3)-PZT (JCPDS card 34-0103 for $Pb(Ni_{0.33}Nb_{0.67})O_3$ and 73-2022 for $Pb(Zr_{0.58}Ti_{0.42})O_3$)

Table 1. Variation of perovskite phase content, density and grain size for three different compositions of 0.5 $Pb(Ni_xNb_{1-x})O_3$-0.5 PZT, where x = 1/3, 1/2 and 2/3

Composition	Perovskite phase content [%]	Density [g/cm^3]	Grain size [μm]
0.5PNN(1/3)-0.5PZT	100	7.22	0.24
0.5PNN(1/2)-0.5PZT	24.2	7.27	1.1
0.5PNN(2/3)-0.5PZT	4.56	6.94	0.7

The scanning electron micrographs (Fig. 2) reveal the surface morphology with uniform distribution of grains having grain size in the 0.2–1.1 μm range. Figure 3 shows the energy dispersive X-ray analysis spectra confirming the presence of all the elements (i.e., Pb, Ni, Nb, Zr, Ti and O) in the composition.

3.2. Dielectric studies

The temperature dependence of dielectric constant (ε') for 0.5 $Pb(Ni_xNb_{1-x})O_3$-0.5 PZT, where x = 1/3, 1/2 and 2/3 for three different frequencies viz., 10 kHz, 100 kHz and 1 MHz is shown in Fig. 4. It is clearly depicted that all three compositions show diffuse phase transitions (DFT) characterized by a broad Curie peak. The wide peak in the temperature dependence of the dielectric constant (ε') with characteristic dispersion observed at all frequencies is associated with the freezing of dipoles [15]. The existence of compositional fluctuations or the substitution of more than one cation in the equivalent crystallographic sites results in microscopic heterogeneity and, thus, distribution of different local Curie points thereby leading to a diffused broad peak [16]. The dielectric constant was found to increase with increase in grain size. This can be attributed to the fact that as the grain size increases, the grain boundary phase gets smaller, favouring the release of the clamping effect of domain walls to some extent [17]. The minimum and maximum values of dielectric constant for three different compositions are given in Table 2. From these values it was observed that when Ni/Nb are doped in equal ratio, the value of ε' is about 293 (at 10 kHz) which is maximum among these three compositions. The value of dielectric constant (ε') obtained in the present case is low compared to the already reported [10,11]. The difference in the value of ε' is due to the different preparation method and composition (higher ε'

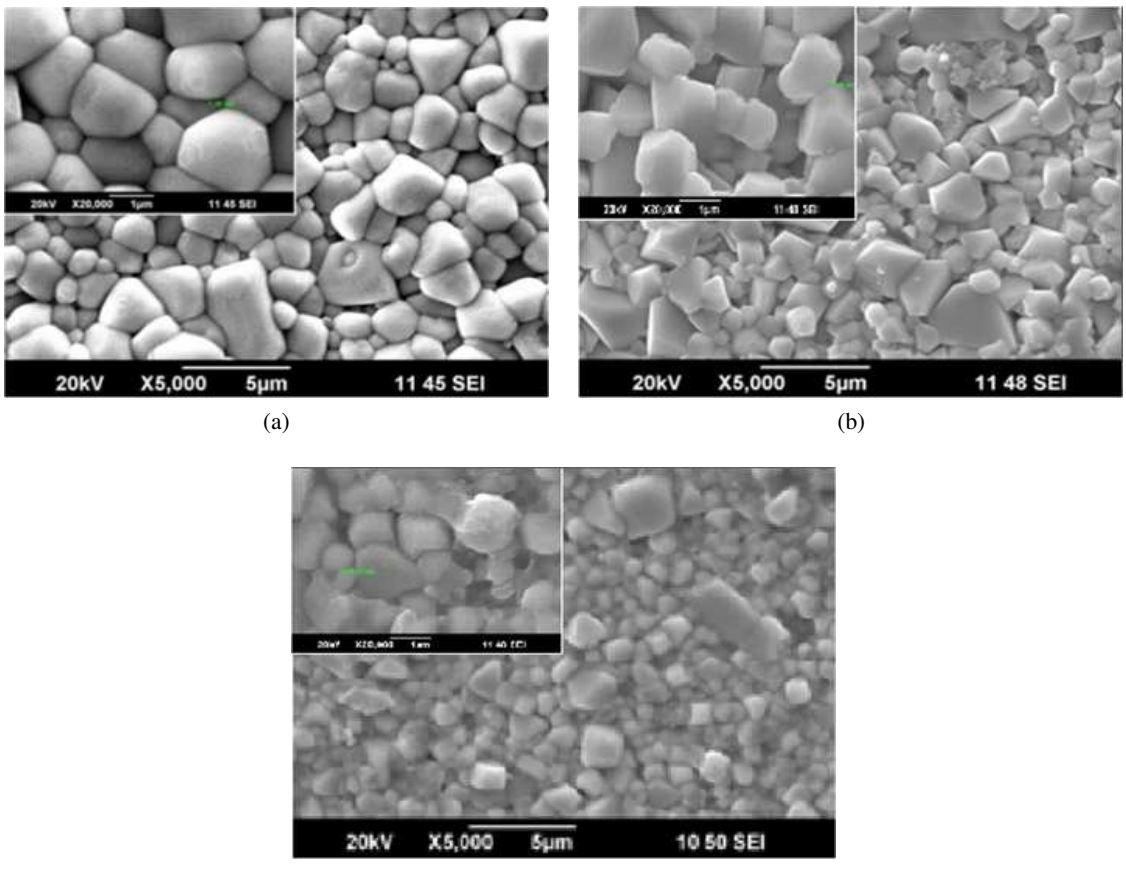

(a) (b)

(c)

Figure 2. Scanning electron micrographs of: a) PNN(1/3)-PZT, b) PNN(1/2)-PZT and c) PNN(2/3)-PZT (inset shows SEM images at higher magnification)

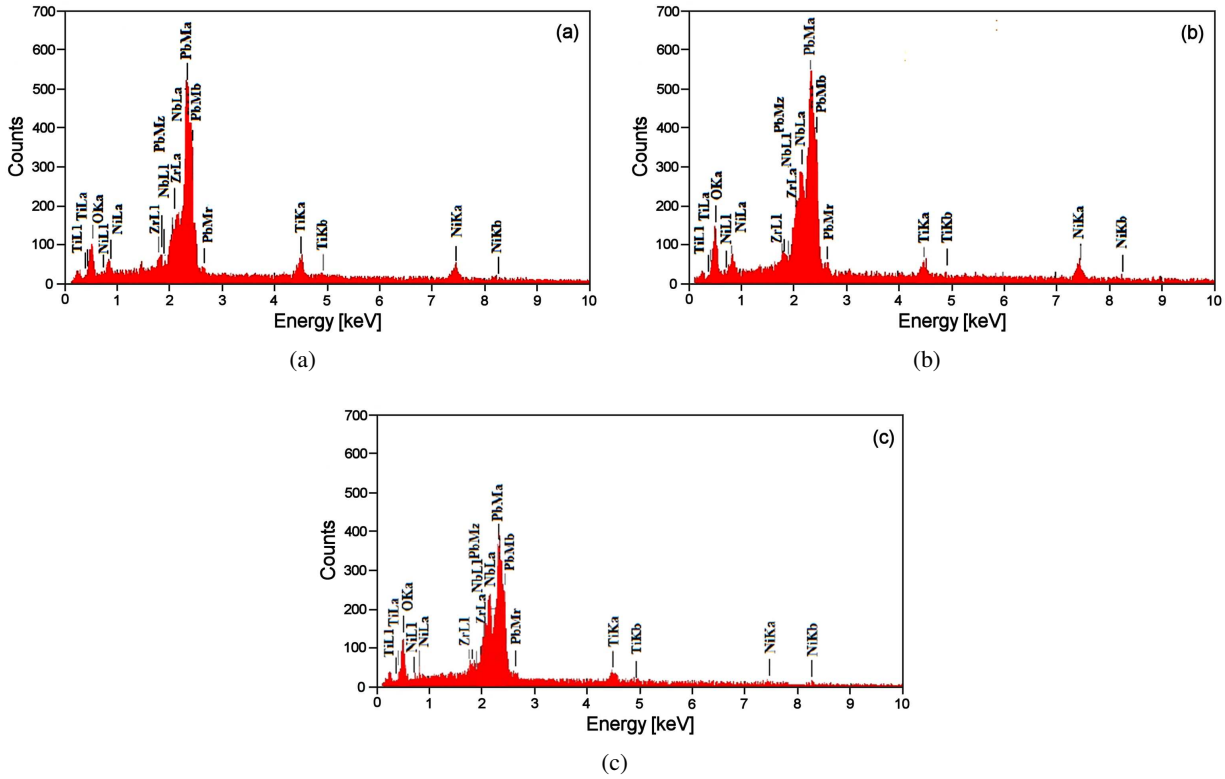

Figure 3. Energy dispersive X-ray analysis results of: a) PNN(1/3)-PZT, b) PNN(1/2)-PZT and c) PNN(2/3)-PZT

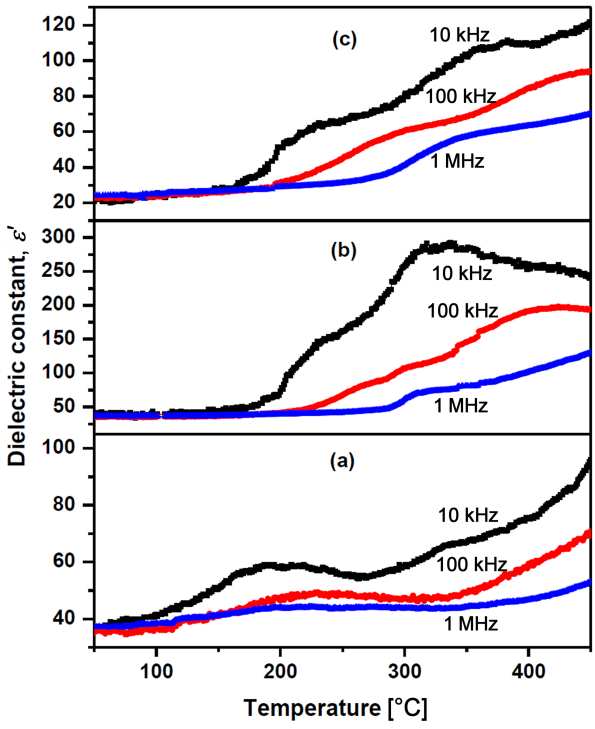

Figure 4. Variation of dielectric constant, ε', with temperature at frequencies of 10 kHz, 100 kHz and 1 MHz for: a) PNN(1/3)-PZT, b) PNN(1/2)-PZT and c) PNN(2/3)-PZT

was obtained for addition of 1 mol% of NiO into PNN-PZT and Zr/Ti = 48/52). Figure 5 shows the frequency dependence of dielectric constant at various temperatures. In all cases, strong frequency dispersion in dielectric constant was observed at lower frequencies followed by nearly frequency independent behaviour at higher frequencies. The value of dielectric constant decreases with increase in frequency and has maximum at lower frequency corresponding to the bulk effect of the system [18]. The decrease in the value of dielectric constant with increasing frequency can be attributed to the electrical relaxation process. Also, the dielectric constant value increases with rise in temperature at all frequencies and this rise in dielectric constant can be attributed to the increase in conduction due to the contribution of space charge polarization [19]. The dielectric losses were obtained only in a particular temperature range shown in Fig. 6 for all three compositions and small peaks can be observed. The shift in peak position towards higher temperature with increasing frequency suggests temperature dependence of dielectric relaxation at selected frequencies. With increase in temperature, the value of $\tan\delta$ also increases, thereby indicating an increase in thermally activated free charge carriers with temperature [20]. PNN(1/3)-PZT possesses lowest dielectric loss and very low loss at lower temperatures and hence possesses good insulating properties.

The nature of dielectric relaxation has been studied through complex plane Argand plot (plot of imaginary part of dielectric constant (ε'') versus real part of dielectric constant (ε')) commonly called Cole-Cole plot [21]. For a purely Debye type process ($\alpha = 0$), the Cole-Cole plot is a perfect semicircle with its centre located on the real axis. However, for non-Debye type relaxation, it is

Table 2. Minimum and maximum values of dielectric constant for three different compositions of 0.5 $Pb(Ni_xNb_{1-x})O_3$-0.5 PZT, where x = 1/3, 1/2 and 2/3

Composition	Minimum value of dielectric constant (ε_{min})	Maximum value of dielectric constant (ε_{max})		
	10 kHz	10 kHz	100 kHz	1 MHz
0.5PNN(1/3)-0.5PZT	37	96	71	53
0.5PNN(1/2)-0.5PZT	35	293	198	129
0.5PNN(2/3)-0.5PZT	20	122	94	70

a distorted semicircle with end points on the real axis and centre lying below the real axis. Mathematically, the Cole-Cole plot obeys the following empirical relation:

$$\varepsilon^* = \frac{\varepsilon_\infty + (\varepsilon_s - \varepsilon_\infty)}{1 + (i\omega\tau)^{1-\alpha}} \quad (2)$$

Here, ε_∞ is the high frequency limit of the permittivity, ε_s is the static dielectric constant, $\varepsilon_s - \varepsilon_\infty$ is the dielectric strength, ω is the angular frequency, τ is the mean relaxation time and α represents distribution of relaxation time which can be determined from the angle subtended by radius of the Cole-Cole plot with the real axis passing through the origin of the imaginary axis. At ε_∞ and ε_s, there will be no dielectric loss and maximum loss occurs at the midpoint between the two dielectric properties values. Figures 7 and 8 depict the Cole-Cole plot for PNN(1/2)-PZT and PNN(2/3)-PZT at two different temperatures, respectively. The data points have been joined by standard polynomial fit. For PNN(1/3)-PZT composition, the losses obtained are in narrow temperature range and also they have very low values, so it was not possible to draw the Cole-Cole plots in this case. Thus, in other two compositions, i.e. PNN(1/2)-PZT and PNN(2/3)-PZT, at low temperatures, the Cole-Cole plot resembles almost straight lines (not shown) with large slopes, suggesting the insulating behaviour of material. But as the temperature increases, the slope of these curves decreases and the curves bend towards the real axis forming semicircles. This suggests an increase in conductivity of the material with rise in temperature. From Figs. 7 and 8 it can be observed that the curves have deformed arcs with their centres located below the real axis thereby confirming the non-Debye type relaxation in such materials. Two semicircular arcs presented in the Cole-Cole plot can be explained on the basis of equivalent circuit containing two parallel RC elements connected in series (Fig. 9), one for bulk crystal (grain) and other for interfacial boundary (grain boundary). Since relaxation time for grain boundary is much larger than that of bulk crystal, arc lying on high frequency range is associated with grain while grain boundary is associated with low frequency region. This indicates negative temperature coefficient of resistance (NTCR) behaviour of 0.5 $Pb(Ni_xNb_{1-x})O_3$-0.5 PZT like that of a semiconducting material.

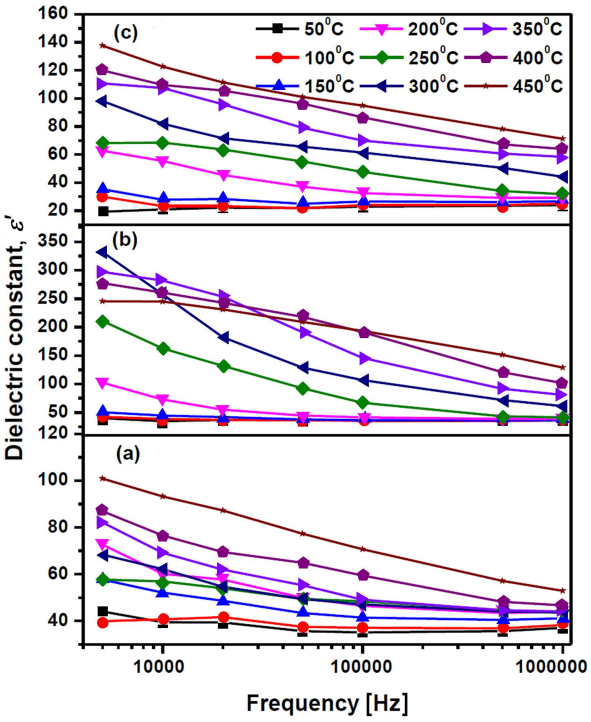

Figure 5. Variation of dielectric constant, ε', with frequency at different temperatures for: a) PNN(1/3)-PZT, b) PNN(1/2)-PZT and c) PNN(2/3)-PZT

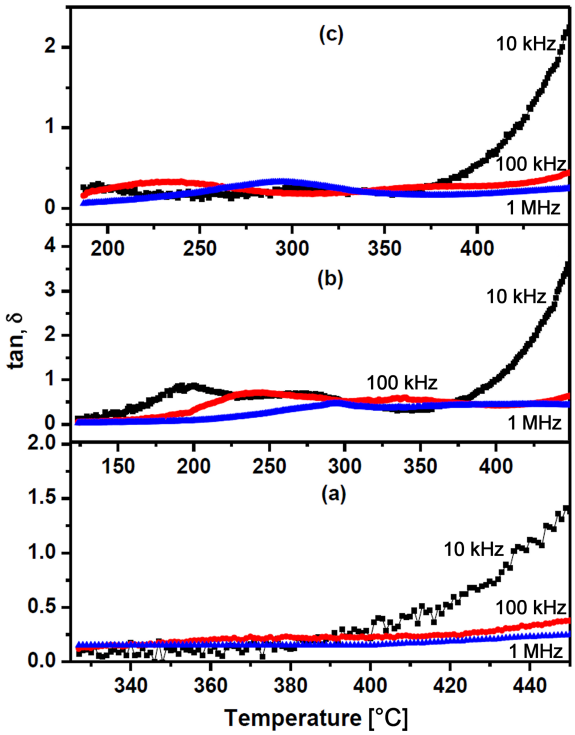

Figure 6. Variation of dielectric loss with temperature at three different frequencies of 10 kHz, 100 kHz and 1 MHz for: a) PNN(1/3)-PZT, b) PNN(1/2)-PZT and c) PNN(2/3)-PZT

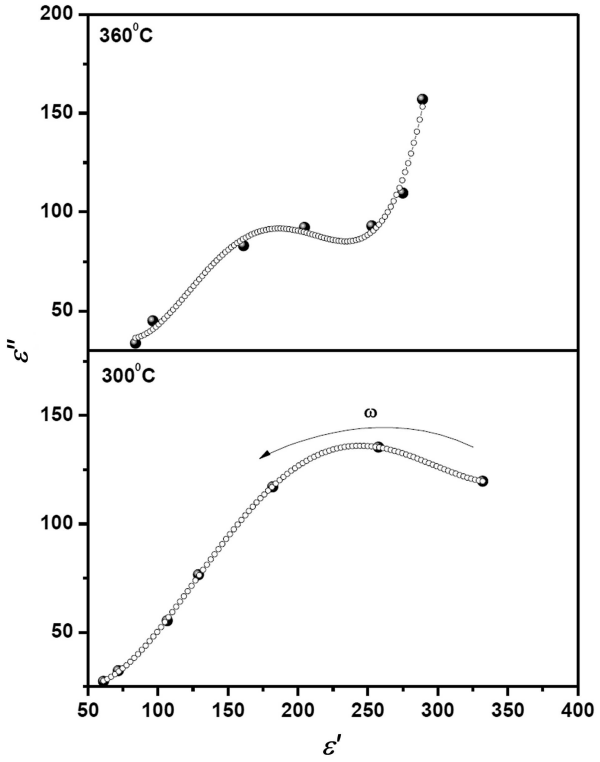

Figure 7. Complex plane Argand plot between imaginary dielectric constant (ε'') and real part of dielectric constant (ε') for PNN(1/2)-PZT at 300 and 360 °C

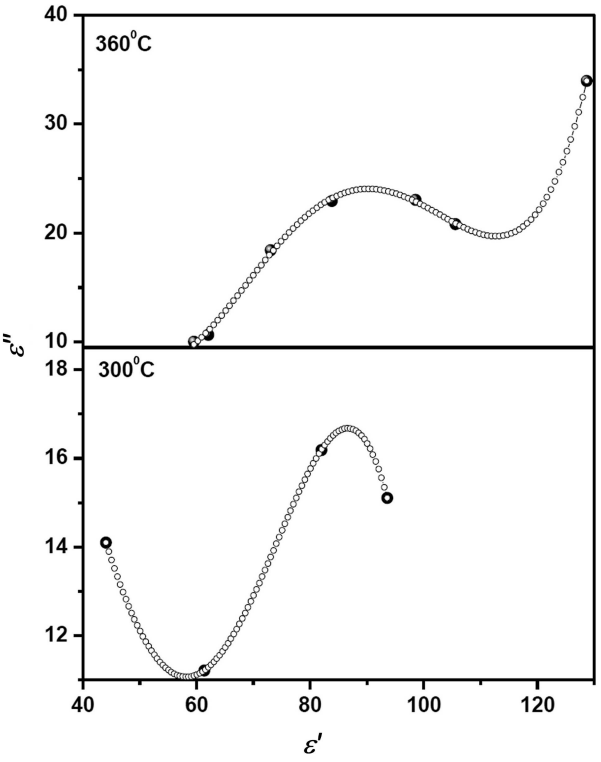

Figure 8. Complex plane Argand plot between ε'' and ε' for PNN(2/3) - PZT at 300 and 360 °C

3.3. AC conductivity and activation energy

AC conductivity (σ_{AC}) has been calculated from dielectric constant (ε') and dielectric loss ($\tan\delta$) data using the empirical relation:

$$\sigma_{AC} = \omega\varepsilon_0\varepsilon' \tan\delta = 2\pi f\varepsilon_0\varepsilon' \tan\delta \qquad (3)$$

where $\varepsilon_0 = 8.845 \times 10^{-12}$ F/m is the permittivity of free space. The variation of AC conductivity as a function of $1000/T$ for frequencies of 10 kHz, 100 kHz and 1 MHz in the temperature range 380–450 °C is shown in Fig. 10. With the increase in frequency, AC conductivity increases. This might be due to the fact that at lower frequencies high energy barriers are present and so the charge carriers contributing to conductivity have high relaxation times, thereby resulting in lower conductivity. However, as the frequency increases, more charge carriers with low barriers heights can respond easily with the applied frequency resulting in higher conductivity. Also an increase in AC conductivity with increase in temperature indicates the negative temperature coefficient of resistance (NTCR) character, thereby suggesting that electrical conduction in this material is due to thermally activated transport process governed by Arrhenius equation:

$$\sigma_{AC} = \sigma_0 \exp\frac{-E_a}{k_B T} \qquad (4)$$

where σ_0 is AC conductivity pre-exponential factor, k_B is the Boltzmann constant and E_a is activation energy. The activation energy calculated from the slope of $\ln(\sigma_{AC})$ versus $1000/T$ graph (Fig. 10) using equation 4 is given in Table 3. From the table, a decreasing trend in activation energy with increasing frequency as well as change in composition was observed. The decrease in activation energy with increasing frequency is attributed to the enhancement of the charge carriers to jump between localized states at higher frequencies of the applied field [22,23]. The activation energy obtained in all cases is < 1 eV and this low value may be due to carrier transport through hopping between localized states in a disordered manner [24,25]. It has been reported in literature [26] that in perovskite oxides, the activation energy for oxygen vacancy migration is ~ 1 eV, whereas for A-site cation migration is ~ 4 eV and for B-site cation migration its value is ~ 14 eV. So, in the present case, the low value of activation energy i.e., < 1 eV suggests the oxygen vacancies to be the most probable hopping carrier. Also, the decrease in activation energy on increasing concentration of Ni is due to the fact that Ni possesses different oxidation states (+1, +2, +3 and +4) and can partially substitute Zr^{4+}, Ti^{4+}

Table 3. Activation energy (E_a) values at different frequencies for three different compositions of 0.5 Pb(Ni_xNb_{1-x})O_3-0.5 PZT, where x = 1/3, 1/2 and 2/3

Composition	Activation energy [eV]		
	10 kHz	100 kHz	1 MHz
0.5PNN(1/3)-0.5PZT	0.51	0.16	0.15
0.5PNN(1/2)-0.5PZT	0.44	0.13	0.12
0.5PNN(2/3)-0.5PZT	0.38	0.08	0.07

Table 4. Variation of remnant polarization (P_r), saturation polarization (P_s) and coercivity (E_c) for three different compositions of 0.5 $Pb(Ni_xNb_{1-x})O_3$-0.5 PZT, where x = 1/3, 1/2 and 2/3

Composition	Remnant polarization [μC/cm^2]	Saturation polarization [μC/cm^2]	Coercivity [kV/cm]
0.5PNN(1/3)-0.5PZT	4.25	7.56	3.94
0.5PNN(1/2)-0.5PZT	-	-	11.51
0.5PNN(2/3)-0.5PZT	0.28	2.68	4.51

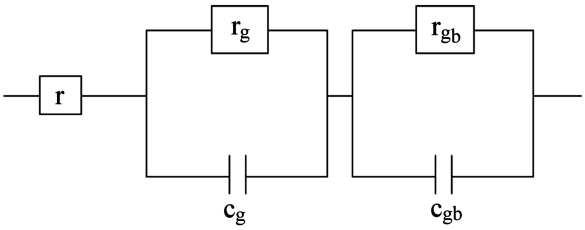

Figure 9. Parallel RC equivalent circuit explaining two semicircles obtained in Cole-Cole plot

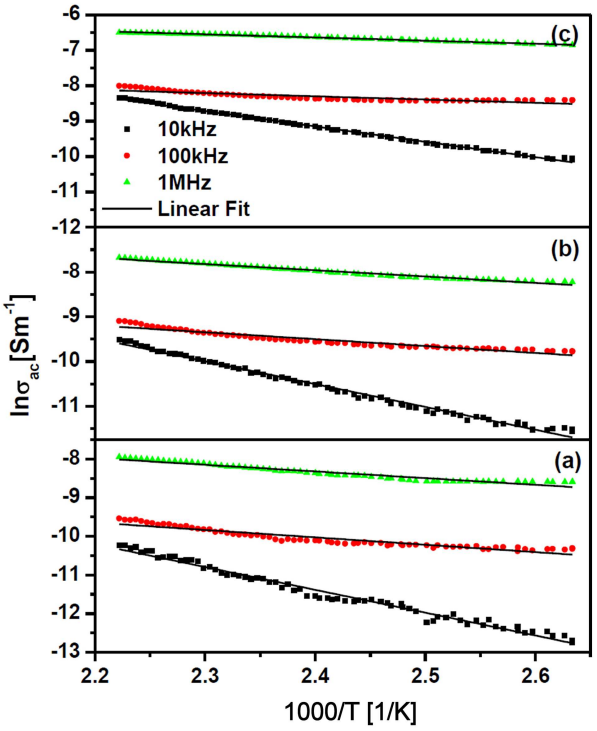

Figure 10. Temperature dependence of the AC conductivity at 10 kHz, 100 kHz and 1 MHz frequency for: a) PNN(1/3)-PZT, b) PNN(1/2)-PZT and c) PNN(2/3)-PZT

and Nb^{5+} thus leading to the creation of oxygen vacancies [27]. While Ni concentration increases, the number of oxygen vacancies also increases and hence activation energy decreases.

3.4. Ferroelectric studies

The polarization versus electric field (*P-E*) hysteresis loops for the PNN-PZT composites with different Ni/Nb ratio, x = 1/3, 1/2 and 2/3 is shown in Fig. 11. The lowest coercive field (E_c = 3.94 kV/cm) and the highest remnant polarization (P_r = 4.25 μC/cm^2) were observed for the composition PNN(1/3)-PZT. A flattened loop was

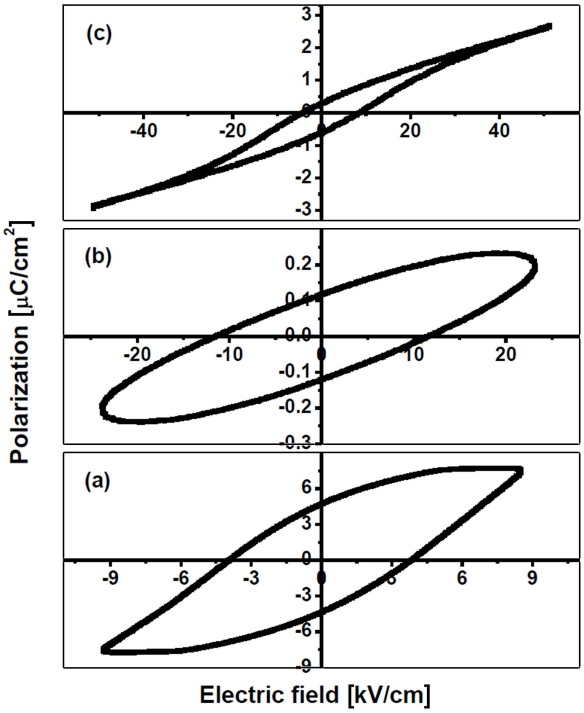

Figure 11. Polarization (P) versus electric field (E) loop for: a) PNN(1/3)-PZT, b) PNN(1/2)-PZT and c) PNN(2/3)-PZT

obtained for composition PNN(1/2)-PZT and no saturation polarization was obtained in this case up to a maximum applied field of 23 kV/cm. A further increase in the applied field led to the electrical breakdown. The unsaturated *P-E* loop obtained in this case may be due to the low resistivity of this sample [28]. Due to leaky nature of the loop, it gives wrong value of remnant polarization. The typical slim *P-E* loop is obtained for the composition PNN(2/3)-PZT. The value of remnant polarization and coercivity is also related to the grain size of the samples. The smallest grain size (0.24 μm) was obtained for PNN(1/3)-PZT and it has maximum value of remnant polarization (4.25 μC/cm^2) and minimum coercivity (3.94 kV/cm). Thus, a direct correlation is obtained between the grain size and the ferroelectric properties. Also, it has been observed that remnant polarization reduces from 4.25 μC/cm^2 for PNN(1/3)-PZT to 0.28 μC/cm^2 for PNN(2/3)-PZT, demonstrating that degree of "switchable" polarization is significantly reduced owing to domain wall clamping. In general, the acceptor doping is accompanied by the generation of oxygen vacancies for ionic charge compensation, which in turn hinders the domain wall motion and lead to the decrease of remnant polarization with simultaneous increase of coercivity [29]. The values of remnant polar-

ization, saturation polarization and coercivity are given in Table 4.

IV. Conclusions

Lead nickel niobate-lead zirconate titanate (PNN-PZT) ceramics having general formula $0.5\,Pb(Ni_xNb_{1-x})O_3$-0.5 PZT, where x = 1/3, 1/2, 2/3 with Zr/Ti = 50/50 were synthesized by conventional mixed oxide route and sintered at 1100 °C. X-ray diffraction analysis confirms the perovskite phase along with pyrochlore phase formation for the samples with x = 1/2 and 2/3 (PNN(1/2)-PZT and PNN(2/3)-PZT). Scanning electron micrographs depict dense and homogeneous packing of grains with average grain size in the sub-micrometer range whereas the presence of almost all elements was confirmed by energy dispersive X-ray analysis (EDAX). The dielectric spectroscopy indicates the highest value of dielectric constant (293) for the composite PNN(1/2)-PZT. The dielectric behaviour indicates formation of diffuse phase transition. The dielectric loss was found to increase with rise in temperature. The temperature dependence of AC conductivity indicates increase in conductivity with increase in temperature thereby suggesting negative temperature coefficient of resistance (NTCR) character. The polydispersive nature of dielectric relaxation is explained on the basis of complex plane Argand plot and its shape indicates the contribution from both grain and grain boundary in the relaxation process. The low value of activation energy (< 1 eV) suggests the oxygen vacancies as the dominant hopping charge carrier. The highest value of remnant polarization was obtained for the composite PNN(1/3)-PZT. Typical ferroelectric loop was obtained for PNN(1/3)-PZT and PNN(2/3)-PZT whereas unsaturated ferroelectric loop was observed in the case of the sample PNN(1/2)-PZT.

Acknowledgement: One of the authors Dr. Deepa Singh is thankful to Department of Science & Technology, Government of India for awarding Women Scientist vide no.: SR/WOS-A/PS-59/2012 (G). The authors express their gratitude to Sophisticated Test and Instrumentation Center (STIC) Cochin University for providing XRD and SEM-EDAX facilities. We are also thankful to Dr. Binay Kumar, Department of Physics, University of Delhi, for providing the facility of *P-E* loop tracer.

References

1. L.E. Cross, "Relaxor ferroelectrics", *Ferroelectrics*, **76** (1987) 241–267.
2. G.R. Shrout, A. Halliyal, "Preparation of lead-based ferroelectric relaxors for capacitors", *Am. Ceram. Soc. Bull.*, **66** (1987) 704–711.
3. K. Uchino, "Electrostrictive actuators: Materials and applications", *Bull. Am. Ceram. Soc.*, **65** [4] (1986) 647–652.
4. L.E. Cross, S.J. Jang, R.E. Newnham, S. Nomura, K. Uchino, "Large electrostrictive effects in relaxor ferroelectrics", *Ferroelectrics*, **23** [3] (1980) 187–192.
5. E.F. Alberta, A.S. Bhalla, "Piezoelectric and dielectric properties of transparent PNNZT ceramics prepared by hot isostatic pressing", *Int. J. Inorg. Mater.*, **3** [7] (2001) 987–995.
6. H. Fan, H.E. Kim, "Preparation and improvement in the electrical properties of lead-zinc-niobate based ceramics by thermal treatments", *J. Mater. Res.*, **17** (2002) 180–185.
7. I.-T. Seo, C.-H. Choi, I.-Y. Kang, S. Nahm, S.B. Kim, D. Song, J. Lee, T.H. Sung, J.-H. Paik, "The high energy density of $Pb(Zr_{1-x}Ti_x)O_3$-$Pb(Ni_{1/3}Nb_{2/3})O_3$ ceramics for piezoelectric energy harvesting devices", *J. Ceram. Process. Res.*, **13** [6] (2012) 739–743.
8. Y. Yamashita, "Piezoelectric properties of niobium doped $[Pb(Sc_{1/2}Nb_{1/2})_{1-x}Ti_x]O_3$ ceramics material near the morphotropic phase boundary", *Jpn. J. Appl. Phys.*, **33** [8] (1994) 4652–4656.
9. D.S. Lee, C.W. Ahn, W. Kim, H.Y. Choi, Y.H. Jeong, J.S. Lee, J.S. Song, B.K. Min, S.J. Jeong, "The sintering behavior and piezoelectric properties of $Pb(Nb_{2/3}Ni_{1/3})O_3$-$PbTiO_3$-$PbZrO_3$ ceramics using two-step calcination", *J. Korean Phys. Soc.*, **42** (2003) S1215–S1219.
10. G. Robert, M.D. Maeder, D. Damjanovic, N. Setter, "Synthesis of lead nickel niobate-lead zirconate titanate solid solutions by a B-site precursor method", *J. Am. Ceram. Soc.*, **84** [12] (2001) 2869–2872.
11. S. Mahajan, C. Prakash, O.P. Thakur, "Piezoelectric properties of $0.5\,(PbNi_{1/3}Nb_{2/3})O_3$-$0.5\,Pb(Zr_{0.32}Ti_{0.68})O_3$ ceramics prepared by solid state reaction and mechanochemical activation-assisted method", *J. Alloys Compd.*, **471** [1-2] (2009) 507–510.
12. O. Babushkin, T. Lindback, J.-C. Luc, J.-Y.M. Leblais, "Reaction sequence in the formation of perovskite $Pb(Zr_{0.48}Ti_{0.52})O_3$-$Pb(Nb_{2/3}Ni_{1/3})O_3$ solid solution: Dynamic heat-treatment", *J. Eur. Ceram. Soc.*, **18** [7] (1998) 737–744.
13. Y.-G. Choi, Y.-J. Son, J.-C. Kweon, K.-W. Cho, Y.-M. Kim, M.-S. Yoon, I.-H. Kim, S.-C. Ur, "The effect of NiO addition to the PNN-PZT piezoelectric ceramics on piezoelectric properties", *Korean J. Mater. Res.*, **15** [6] (2005) 413–418.
14. Yi-Ch. Liou, "Effect of heating rate on properties of $Pb(Fe_{1/2}Nb_{1/2})O_3$ ceramics produced by simplified wolframite route", *Ceram. Int.*, **30** (2004) 567–569.
15. A.A. Bokov, Z.-G. Ye, "Recent progress in relaxor ferroelectrics with perovskite structure", *J. Mater. Sci.*, **41** (2006) 31–52.
16. G.A. Smolenskii, "Physical phenomena in ferroelectrics with diffused phase transition", *J. Phys. Soc. Jpn.*, **28** [1] (1970) 26–37.
17. C.A. Randall, A.D. Hilton, D.J. Barber, T.R. Shrout, "Extrinsic contributions to the grain-size dependence

of relaxor ferroelectric $Pb(Zn_{1/3}Nb_{2/3})O_3$-$PbTiO_3$ ceramics", *J. Mater. Res.*, **8** (1993) 880–884.
18. D.K. Mahato, A. Dutta, T.P. Sinha, "Dielectric relaxation and ac conductivity of double perovskite oxide Ho_2ZnZrO_6", *Phys. B: Condensed Matter*, **406** [13] (2011) 2703–2708.
19. V. Gupta, K.K. Bamzai, P.N. Kotru, B.M. Wanklyn, "Dielectric properties, ac conductivity and thermal behavior of flux grown cadmium titanate crystals", *Mater. Sci. Eng. B*, **130** (2006) 163–172.
20. I. Levin, J.Y. Chan, J.E. Maslar, T.A. Vanderah, "Phase transitions and microwave dielectric properties in the perovskite-like $Ca(Al_{0.5}Nb_{0.5})O_3$-$CaTiO_3$ system", *J. Appl. Phys.*, **90** [2] (2001) 904–914.
21. K.S. Cole, R.H. Cole, "Dispersion and absorption in dielectrics I. Alternating current characteristics", *J. Chem. Phys.*, **9** (1941) 341–351.
22. A.A. Ebnalwaled, "On the conduction mechanism of p-type GaSb bulk crystal", *Mater. Sci. Eng. B*, **174** (2010) 285–289.
23. N.A. Hegab, M.A. Afifi, H.E. Atyia, A.S. Farid, "AC conductivity and dielectric properties of amorphous $Se_{80}Te_{20-x}Ge_x$ chalcogenide glass film compositions", *J. Alloys Compd.*, **477** (2009) 925–930.
24. S. Upadhyay, A.K. Sahu, D. Kumar, O. Parkash, "Probing electrical conduction behavior of $BaSnO_3$", *J. Appl. Phys.*, **84** (1998) 828–832.
25. K. Prasad, C.K. Suman, R.N.P. Choudhary. "Electrical characterization of $Pb_2Bi_3SmTi_5O_{18}$ ceramic using impedance spectroscopy", *Adv. Appl. Ceram.*, **105** (2006) 258–264.
26. M.S. Islam, "Ionic transport in ABO_3 perovskite oxides: A computer modelling tour", *J. Mater. Chem.*, **10** (2000) 1027–1038.
27. M. Zheng, Y. Hou, M. Zhu, M. Zhang, H. Yan, "Comparitive study of microstructure, electric properties and conductivity for NiO and PNN modified $Pb(Zn_{1/3}Nb_{2/3})O_3$-$PbZrO_3$-$PbTiO_3$ ceramics", *Mater. Res. Bull.*, **51** (2014) 426–431.
28. A.K. Roy, A. Singh, K. Kumari, K.A. Nath, A. Prasad, K. Prasad, "Electrical properties and AC conductivity of $(Bi_{0.5}Na_{0.5})_{0.94}Ba_{0.06}TiO_3$ ceramic", *ISRN Ceram.*, **2012** (2012) 1–10.
29. S. Zhang, S.M. Lee, D.H. Kim, H.Y. Lee, T.R. Shrout, "Characterization of Mn-modified $Pb(Zn_{1/3}Nb_{2/3})O_3$-$PbZrO_3$-$PbTiO_3$ single crystals for high power broad bandwidth transducers", *Appl. Phys. Lett.*, **93** (2008) 122908.